Journal of Theoretical Biology 382 (2015) 284–291

Contents lists available at ScienceDirect

Journal of Theoretical Biology

journal homepage: www.elsevier.com/locate/yjtbi

Tooth germ invagination from cell–cell interaction: Working hypothesis on mechanical instability

Hisako Takigawa-Imamura [a,1], Ritsuko Morita [b,2], Takafumi Iwaki [c,3], Takashi Tsuji [b,4], Kenichi Yoshikawa [a,d,*]

[a] Department of Physics, Graduate School of Science, Kyoto University, Kitashirakawa-Oiwake, Sakyo-ku, Kyoto 606-8502, Japan
[b] Research Institute for Science and Technology, Tokyo University of Science, 2641Yamazaki, Noda, Chiba 278-8510, Japan
[c] Fukui Institute for Fundamental Chemistry, Kyoto University, 34-4 Takano-Nishihiraki-cho, Sakyo-ku, Kyoto 606-8103, Japan
[d] Faculty of Life and Medical Sciences, Doshisha University, 1-3 Tatara Miyakodani, Kyotanabe, Kyoto 610-0394, Japan

HIGHLIGHTS

- We model epithelial invagination of the early tooth germ.
- Cell-cell mechanical interaction is considered in an abstract tissue geometry.
- Epithelial buckling occurs by mechanical stress of growing.
- An unknown significance of histological features in tooth development is proposed.

GRAPHICAL ABSTRACT

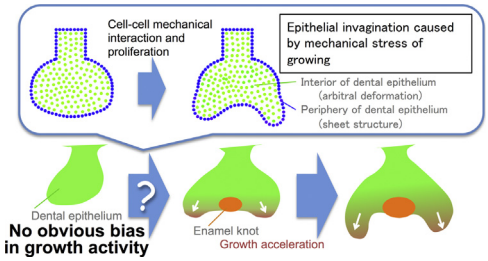

ARTICLE INFO

Article history:
Received 5 November 2014
Received in revised form
5 July 2015
Accepted 8 July 2015
Available online 17 July 2015

Keywords:
Morphogenesis
Buckling
Epithelium

ABSTRACT

In the early stage of tooth germ development, the bud of the dental epithelium is invaginated by the underlying mesenchyme, resulting in the formation of a cap-like folded shape. This bud-to-cap transition plays a critical role in determining the steric design of the tooth. The epithelial-mesenchymal interaction within a tooth germ is essential for mediating the bud-to-cap transition. Here, we present a theoretical model to describe the autonomous process of the morphological transition, in which we introduce mechanical interactions among cells. Based on our observations, we assumed that peripheral cells of the dental epithelium bound tightly to each other to form an elastic sheet, and mesenchymal cells that covered the tooth germ would restrict its growth. By considering the time-dependent growth of cells, we were able to numerically show that the epithelium within the tooth germ buckled spontaneously, which is reminiscent of the cap-stage form. The difference in growth rates between the peripheral and interior parts of the dental epithelium, together with the steric size of the

* Corresponding author at: Faculty of Life and Medical Sciences, Doshisha University, 1-3 Tatara, Miyakodani, Kyotanabe, Kyoto 610-0394, Japan.
E-mail address: keyoshik@mail.doshisha.ac.jp (K. Yoshikawa).
[1] Anatomy and Cell Biology, Graduate School of Medical Sciences, Kyushu University, 3-1-1 Maidashi, Higashi-ku, Fukuoka 812-8582, Japan.
[2] Laboratory for Tissue Microenvironment, RIKEN Center for Developmental Biology, 2-2-3 Minatojima-minamimachi, Chuo-ku, Kobe, Hyogo 650-0047, Japan.
[3] Physics, Faculty of Medicine, Oita University, 1-1 Idaigaoka, Hasama-machi, Yufu, Oita 879-5593, Japan.
[4] Laboratory for Organ Regeneration, RIKEN Center for Developmental Biology, 2-2-3 Minatojima-minamimachi, Chuo-ku, Kobe, Hyogo 650-0047, Japan.

http://dx.doi.org/10.1016/j.jtbi.2015.07.006

tooth germ, were determining factors for the number of invaginations. Our theoretical results provide a new hypothesis to explain the histological features of the tooth germ.

1. Introduction

Morphogenesis is an autonomous process in tissues that occurs during the growth of multicellular organisms. A layered structure composed of regularly arrayed cells, which is called the epithelium, contours each organ throughout the body (Gilbert, 2006). Morphogenetic events are often accompanied by epithelial deformation, as in gastrulation, ectodermal placode formation, lung branching, and intestinal villi formation (Chuong and Noveen, 1999; Sweeton et al., 1991). It has been considered that a specific shape arises due to local differences in cellular behavior controlled by signaling molecules. In addition to this common morphogenetic concept, models of spontaneous deformation based on mechanical cell–cell interaction are expected to lead to breakthroughs in our understanding of large-scale shape changes (Bilder and Haigo, 2012; Drasdo and Forgacs, 2000; Hočevar Brezavšček et al., 2012; Ishihara and Sugimura, 2012; Nagai and Honda, 2001; Sherrard et al., 2010; Sweeton et al., 1991).

Organogenesis of ectodermal organs, such as teeth (Fig. S1 and Text S1 in the Supporting material), hair, and the optic cup, involves a large-scale deformation process that is critical for later development (Eiraku et al., 2011; Jernvall et al., 1994; Paus et al., 1999; Toyoshima et al., 2012; Vaahtokari et al., 1996). In the early stage of tooth development, a bud of dental epithelium grows into a cap structure with an invaginated tip (Fig. 1A, white arrowhead). This step is called the bud-to-cap transition (Fig. 1A and B, from the middle to the lower panels) and begins the process that determines the cell fate depending on positional relationships. It has also been shown that the cap structure determines the shape and unit of the tooth, based on the fact that a tooth germ with multiple invaginations ultimately forms multicusped teeth or even extra teeth *in vitro* (Cai et al., 2007; Harjunmaa et al., 2012; Nakao et al., 2007) and *in vivo* (Järvinen et al., 2006; Nakamura et al., 2008). Despite the importance of the formation of the cap structure in tooth morphogenesis, there have been no theoretical studies on this process, while tooth alignment (Kulesa et al., 1995) and cusp formation (Osborn, 2008; Salazar-Ciudad and Jernvall, 2002) have been modeled.

The progress of the bud-to-cap transition has been considered to be directed by mutual regulation between the epithelium and mesenchyme via chemical signaling, such as by FGFs, SHH, WNTs and BMPs (Thesleff, 2003; Tucker and Sharpe, 2004). Especially, a signaling center called the enamel knot is thought to play a pivotal role in tooth development (Fig. 1B, lower panel). It has been considered that convex and concave regions of the cap-stage dental epithelium are the result of differential growth via diffusive signals from the primary enamel knot (Jernvall et al., 1994; Tucker and Sharpe, 2004). However, enamel knot-related genes are expressed only faintly before the cap stage (http://bite-it.helsinki.fi) (Jernvall et al., 1998; Vaahtokari et al., 1996), and the causal relationship between the enamel knot and the bud-to-cap transition is still not clear. As shown in Fig. S1B, it has become evident that the local amplification of proliferation activities is not significant in the early tooth germ before invagination (E13.5 and E14.0), in contrast to the evident regional bias in E14.5. This implies that the morphogen gradient plays only a minor role in the early stage. Thus, as the first step in elucidating the mechanism of the bud-to-cap transition, we performed a numerical study on the effect of mechanical instability on morphogenesis.

To consider the mechanism of the bud-to-cap transition, we focused on the histological features of the bud-stage tooth germ (Fig. 1) (Lesot and Brook, 2009). As we demonstrated in Fig. 1A, the interior cells of the epithelial bud do not show consistent alignment. On the other hand, the peripheral cells of the epithelial bud are aligned densely along the basement membrane (Lesot and Brook, 2009). These facts imply the presence of different adherence properties between the cells in the interior and periphery. It has been reported that the expressions of E- and P-cadherin differ between the interior and periphery from the bud stage (Palacios et al., 1995). After the cap stage, the interior part of the dental epithelium is histologically discriminated from the periphery as *stellate reticulum* (Lesot and Brook, 2009; Sasaki et al., 1984; Thesleff et al., 1996). Regardless of these studies, to the best of our knowledge, no previous report seems to have addressed the possible significance of the different cell modes in the epithelial bud before the cap stage for tooth development. In addition, little attention has been given to the finding that the boundary of the dental mesenchyme and the oral mesenchyme starts to form a collagen type IV-rich fibrous barrier, which we tentatively call the multifiber layer, from the bud stage (Fig. 1A) (Fukumoto et al., 2006; Mammoto et al., 2011; Yoshiba et al., 2003). Fig. 1A shows that the dental mesenchymal cells exhibit compressed shapes along the direction of the multifiber layer, which may provide information to estimate the force field (Ishihara and Sugimura, 2012). Actually, a compaction experiment implied that the dental mesenchyme is under pressure in the tooth germ (Mammoto et al., 2011).

In this study, we investigated the mechanism of the bud-to-cap transition in tooth development. We presume that epithelial folding is induced through mechanical force that is spontaneously generated by cell growth in the dental epithelium. Our model links the histological features of the tooth germ and cellular behavior to the mechanism of shape formation. The purpose of the present study was to consider the possible role of mechanical instability in relation to a difference in the cell population in the mechanism of tooth development, based on experimental observations (Jernvall and Thesleff, 2000; Jussila and Thesleff, 2012; Pispa and Thesleff, 2003). We propose a new hypothesis regarding cap shape formation under a simple theoretical framework that does not involve directed cell motion or signal distribution.

2. Materials and methods

2.1. Animals

C57BL/6 mice were purchased from SLC, Inc. (Shizuoka, Japan). R26R-Lyn-Venus mice (CDB Acc. no. CDB0219K at http://www.cdb.riken.jp/arg/mutant%20mice%20list.html) were obtained from the RIKEN CDB Laboratory for Animal Resources and Genetic Engineering (Hyogo, Japan) (Abe et al., 2011). All mouse care and handling complied with the NIH guidelines for animal research. All experimental protocols were approved by the Animal Care and Use Committee of Tokyo University of Science.

2.2. Histochemical analysis and immunohistochemistry

The tissues were removed and immersed in 4% paraformaldehyde in PBS(−) for 2–16 h at 4 °C. For histochemical tissue analyses, after fixation, the tissues were embedded in paraffin and sectioned at 5–10 μm. For the storage of frozen samples, the specimens were immersed in a series of graded sucrose solutions and embedded in

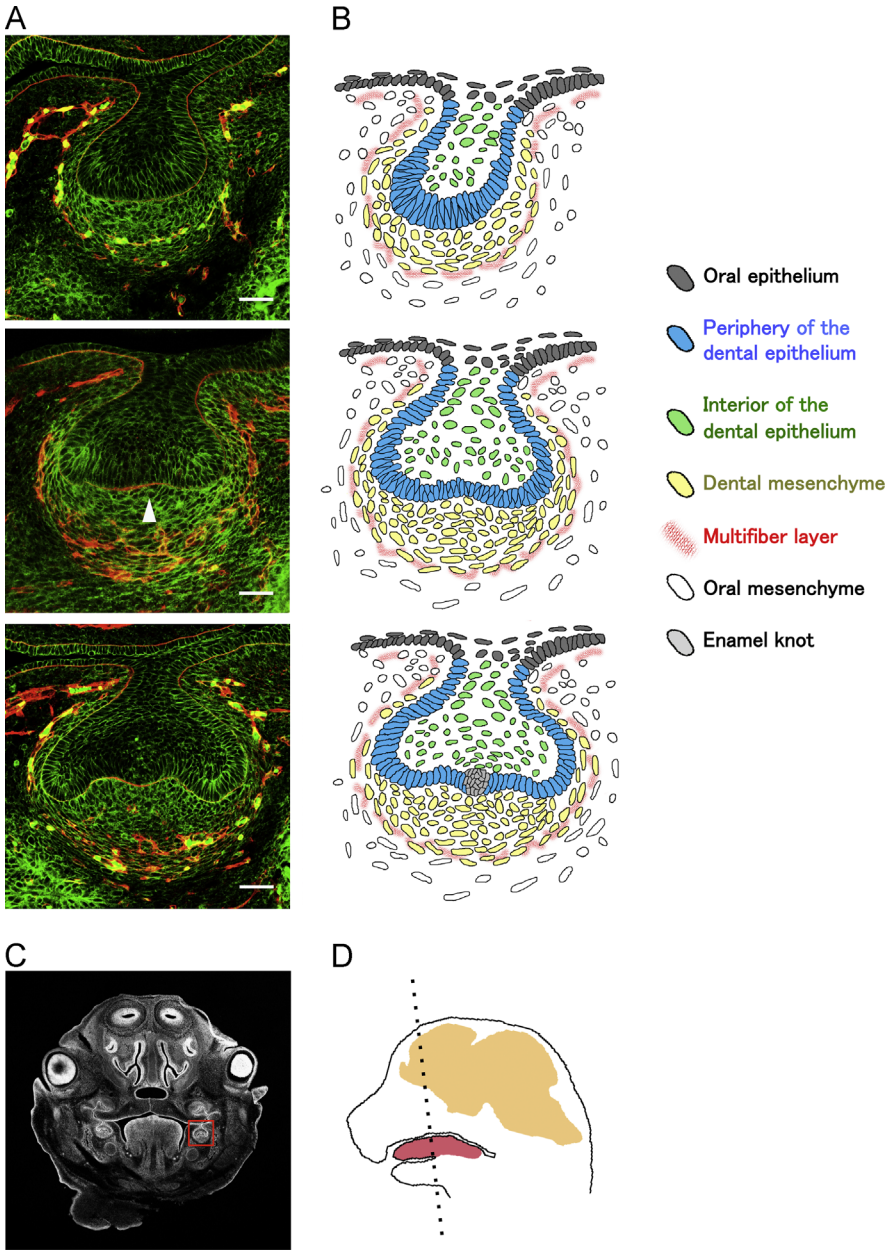

Fig. 1. The bud-to-cap transition of the tooth germ. (**A**) Frontal sections of tooth germs of R26R-Lyn-Venus transgenic mice in which all cell membranes are visualized (Abe et al., 2011). The upper, middle, and lower panels are from mouse embryos on embryonic day 13.5 (E13.5), E14, and E14.5, respectively. Green signals indicate cell membranes. Red signals represent collagen type IV immunostaining, which is a sign of what we tentatively call the multifiber layer. Merged signals (represented in yellow) are intrinsic fluorescence from blood cells. White arrowhead indicates the invaginated tip of the dental epithelium. Scale bar = 50 μm. (**B**) Schematic representations of each panel in (A). The distinct cell colors represent different cell types. (**C, D**) Overview of the mouse sections shown in (A). (**C**) Frontal section of the head of an R26R-Lyn-Venus transgenic mouse. A red box indicates a magnified area in (A). (**D**) Schematic drawing of a midsagittal section of the head. The frontal section plane used for (C) is indicated by dashed lines. Orange and red areas indicate the brain and tongue, respectively. (For interpretation of the references to color in this figure legend, the reader is referred to the web version of this article).

Tissue-Tek O.C.T. (Sakura-Finetek USA, Torrance, *CA*). For immunohistochemistry, Anti-Collagen Type IV (1:200, Millipore, Temecula, *CA*) polyclonal antibody was used. Immunoreactivity was detected using Alexa Fluor® 647 Donkey Anti-Rabbit IgG (H+L) Antibody (1:500, Molecular Probes, Eugene, OR). All fluorescence microscopy images were captured under a confocal microscope (LSM780, Carl Zeiss).

2.3. Numerical calculation

The source code was written in C++ based on the open source code for Smoothed Particle Hydrodynamics (https://github.com/takagi/blog-codes/blob/master/20090223/sph.cpp), which calculates the interactions among many particles efficiently.

3. Results

3.1. Model

The essence of our hypothesis is that the ratio of the growth of the epithelial sheet to the increase in the volume of the epithelium plays an essential role in the stability of shape. Based on the differences in shape and adherence properties between the peripheral and interior cells (Fig. 1A), we assumed that the periphery and the interior are composed of distinct cell types (Fig. 1B) and that they do not mix with each other. Let us consider a spherical tissue in which the periphery and interior are composed of different assemblies. When both the peripheral and

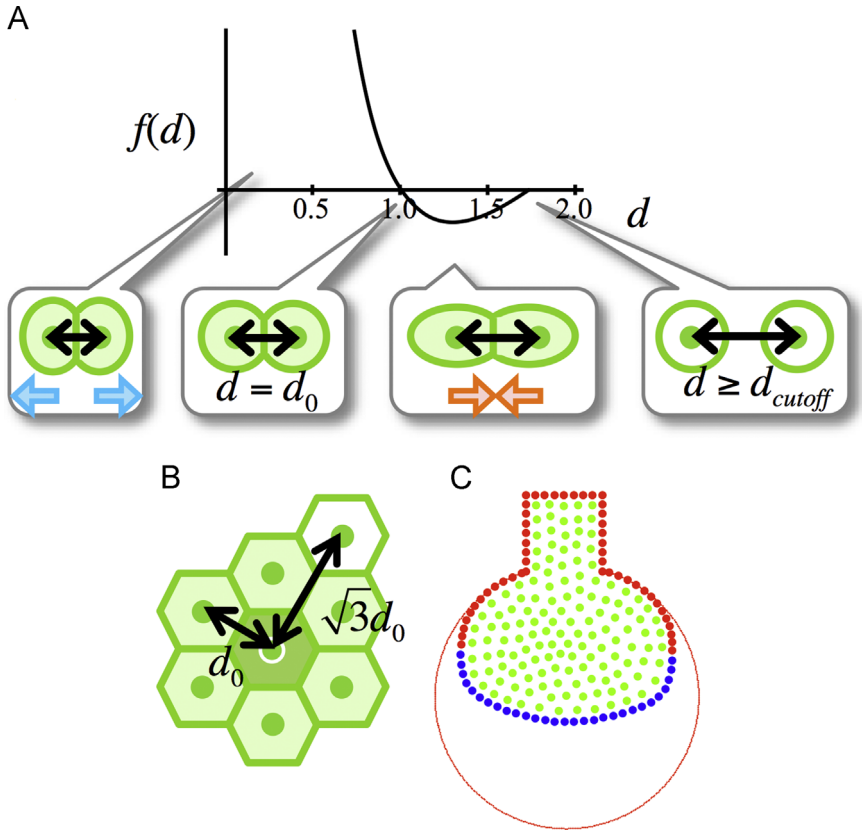

Fig. 2. The model's framework. (**A**) Force acting between a pair of particles in the basic dynamics (see Appendix A). Repulsive and attractive forces are present when the distance between particles is shorter and longer than the optimal distance $d_0 = 1$, respectively. The relative cutoff distance is set to be $d_{cutoff}^{interior} = 3^{1/2}$ (**B**) The concept of the cutoff distance. The cutoff distance was set to be the minimum distance between a non-adjacent pair of particles in the close-packed lattice. (**C**) Layout of particles in the numerical simulation. Blue and green dots (gray and light gray dots in monochrome images) represent the centers of peripheral and interior epithelial particles, respectively. Red dots (dark gray dots in monochrome images) represent the centers of fixed peripheral particles that form an elastic layer with the blue peripheral particles. The number of particles was determined based on the number of cells seen in a frontal section of the tooth bud. The red line indicates a fixed wall, which designates the multifiber layer.

interior cells proliferate at the same rate, the tissue's surface S will not scale linearly with the tissue's volume V, since S–$V^{2/3}$ for a sphere. The disproportion between the periphery (S) and interior (V) generates mechanical force to restore the stability of the shape. Deformation from a round shape to an irregular shape will resolve the imbalance in the surface–volume ratio.

To depict this concept in the growth process, we constructed a mechanical model of cell motion (Fig. 2). The cellular dynamics are based on the intuition that early tooth development is governed by the principle that a cell tends to move from a more crowded space to a less crowded space. We applied center dynamics, which are simple and sufficient to examine this idea, and do not consider the change in cell shape for simplicity. Each cell is assumed to be a particle, and is represented by a mass point positioned at the center of the particle. Cell–cell binding and retention of the cell volume are simply interpreted in terms of the mechanical interaction between neighboring particles.

Mechanical interaction is assumed to be determined by the distance d between cell centers (Fig. 2A, Appendix A). The ideal distance between a pair of cells d_0 was defined as the resting state. Both repulsive ($d < d_0$) and attractive ($d > d_0$) interactions are present, and each cell moves in response to the sum of these interactions. We set a cutoff distance, d_{cutoff}, at which interaction is lost (Fig. 2B). This corresponds to the case when the cells are far enough apart from each other to lose direct contact. We also assumed that cell division occurs under a constant probability within the same type of cells (Appendix B).

The particles were arranged to construct the tooth germ model (Fig. 2C). Without losing generality, we adopted a two-dimensional model by considering the shape of the tooth germ in a frontal section (Fig. 1). The peripheral and interior parts of the dental epithelium were considered to be comprised of different assemblies and to behave differently, and the multifiber layer was included in the model (Fig. 2C). We assumed that mesenchyme-like interior epithelial cells behave like free adhesive particles that follow the basic dynamics defined in Appendix A (green dots in Fig. 2C). The peripheral cells also follow the basic dynamics, but maintain a sheet structure that contours the dental epithelium (blue dots in Fig. 2C). For modeling of the sheet structure, the cutoff distance for interaction between an adjacent pair of peripheral cells was set to $d_{cutoff}^{adjacent} = 300$ so that they remained in contact. To retain smooth layering of the peripheral cells on the basement membrane as seen in Fig. 1A, the peripheral layer was interpreted by incorporating the effect of bending elasticity (Appendix C). We assumed that the peripheral and interior cells actively proliferate, based on the expression of the proliferation marker Ki-67 in the dental epithelium (Fig. S1B). We paid attention to the change in shape of the lower side of the dental epithelium under the approximation that the displacement of the peripheral cells on the upper side is negligibly small, according to our observations. Therefore, the positions of the peripheral cells on the upper side were fixed (red dots in Fig. 2C).

We considered the short period of time from the last minute to the beginning of epithelial folding. Therefore, the tooth-germ size was assumed to be nearly constant, and the multifiber layer was modeled as a fixed wall. It is plausible that the multifiber layer affects cellular movement since the thick condensation of extracellular matrices should affect cell–cell binding. We assumed that the dental epithelium and mesenchyme are compressed inside the multifiber layer, based on observations (Fig. 1A) (Mammoto

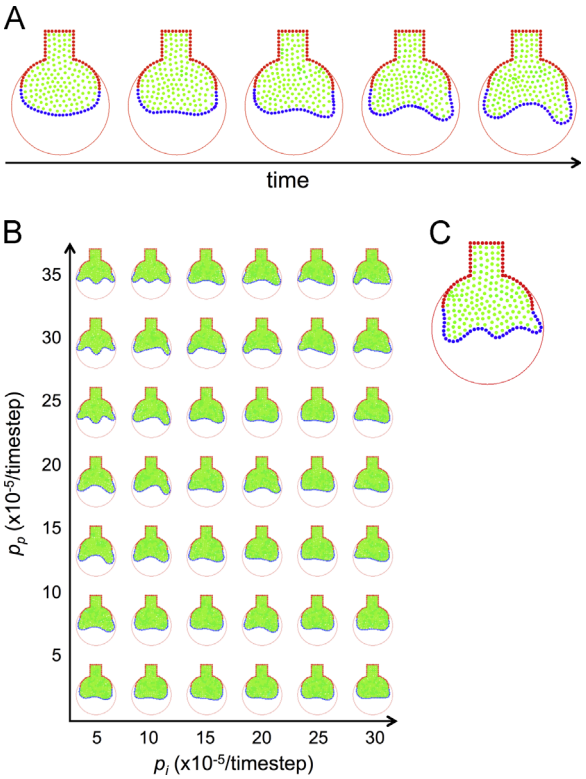

Fig. 3. Autonomous deformation of the tooth germ. (**A**) Example of the results of numerical simulations. Snapshots at time points $t=0$, 6000, 12,000, 18,000, and 24,000 are shown. Parameter values were taken to be $k_{ii}=10$, $k_{ip}=20$, $d^{perif}_{cutoff}=300$, $k_{pp}=0.0024$, $k_{bend}=140$, $\gamma=10$, $p_i=0.00005$, and $p_p=0.00015$ (see Appendixes A, B, and C). Circles with slightly different colors (slightly different tones in monochrome images) indicate newly added particles. The time-development for this result is shown in the Supporting Information (Movie S1). (**B**) Results obtained by changing the proliferation rates for peripheral and interior cells. The process was iterated until the number of interior particles reached 170 or that of peripheral particles reached 90. (**C**) Multiple invaginations seen for the soft peripheral layer. $k_{pp}=120$, $k_{bend}=70$.

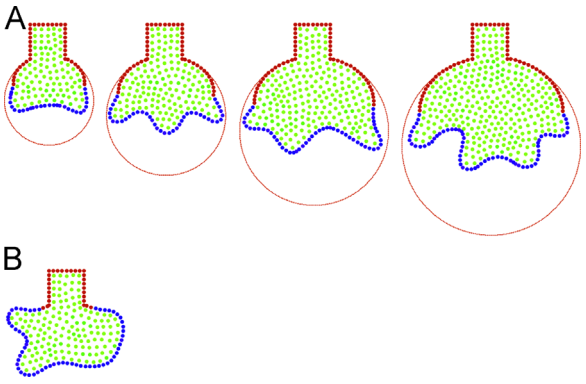

Fig. 4. Irregular shape generation. (**A**) Dependence of the number of folds on the size of the tooth germ. The multifiber layers have radii of 6, 8, 10, and 12. The process was iterated 20,000 times. Parameters were set as in Fig. 3A, except that $p_p=0.00030$. (**B**) Irregular form obtained in the absence of a multifiber layer. Parameters were set as in Fig. 3A.

et al., 2011). We omitted the dental mesenchyme in the present model based on the fact that mesenchymal proliferation is not apparently active before epithelial invagination (Fig. S1B), suggesting that the dental mesenchyme plays only a small role in the initial process of invagination. By adopting a simple model geometry, we focused on the spontaneous change in the shape of the dental epithelium. This simplification was also based on our examination of the model's framework with extensive geometries including the dental mesenchyme, where the parameters that were critical for the shape change were those of the dental epithelium (data not shown).

3.2. Results of the numerical simulation

Fig. 3A and Movie S1 show the invaginated deformation of the modeled dental epithelium during its growth. We examined the effect of the difference in growth rates between the peripheral (p_p) and interior (p_i) cells on epithelial invagination. The results showed that folding was critically dependent on the ratio between p_p and p_i, and did not occur when p_p/p_i was small, which confirms our idea that an imbalance between the periphery and internal parts resulted in the deformation from a round shape (Fig. 3B). A single folding at the lower center of the dental epithelium occurred over a wide range of parameter values, which reflects the robustness of this buckling-driven shape change. Interestingly, multiple folds appeared when p_p/p_i was large, suggesting that the difference in the growth rates is crucial for the regulation of the change in shape. Multiple folds were also generated when the layer elasticity defined by k_{bend} was decreased (Fig. 3C), indicating that elasticity influences the range of the characteristic wavelength.

The dependency on the size of the tooth-germ is shown in Fig. 4A. More folds were seen for a larger tooth germ when there were no changes in the values for p_p and p_i. The folding pattern became more irregular when the multifiber layer was removed (Fig. 4B), suggesting that the multifiber layer makes an important contribution to the bud-to-cap transition.

4. Discussion

We have presented a theoretical model for the bud-to-cap transition of tooth germ. Based on the current biological insights, we adopted a simple model geometry that contained only the essential components to stress the idea that tissue deformation is driven by self-organized epithelial buckling. The difference between growth at the periphery and in the interior leads to buckling of the dental epithelium. The model of invagination is regulated by the growth rates of the peripheral and interior parts and by the size of the tooth germ. The spatial restraint imposed by the multifiber layer provides consistency to the deformed shape.

The underlying concept of our model is in contrast to the traditional perspective that non-proliferating regions are invaginated and proliferating regions protrude, as modeled by Salazar-Ciudad and Jernvall (2010, 2002) (Jernvall and Thesleff, 2000). Our model is similar to Osborn's model of tooth cusp formation, in which shape formation can be explained by epithelial buckling (Osborn, 2008). Here, we considered the initial bud-to-cap transition, and thus focus on a different stage of morphogenesis than in past modeling studies that have focused on the cap stage onward. Our concept is expected to be reasonable as the first theoretical model of the early tooth germ, for which there seems to have been no clear experimental evidence on the active role of morphogen gradients (Fig. S1B) (Jernvall and Thesleff, 2000; Jussila and Thesleff, 2012; Pispa and Thesleff, 2003). The present study stresses the importance of mechanical instability, in addition to the current understanding of the contribution of chemical signaling to the bud-to-cap transition. Invagination of the dental epithelium occurs at the presumptive enamel knot expressing SHH (Dassule et al., 2000; Gritli-Linde, 2002; Hardcastle et al., 1998) and FGF4 (Jernvall et al., 1994; Kettunen et al., 1998; Klein et al., 2006; Kratochwil et al., 2002), which should induce cellular proliferation during development of the tooth germ. It is expected that both the chemical signaling and mechanical influence

work in a cooperative manner to generate epithelial invagination *in vivo*.

Before formation of the cap shape, the dental epithelium has been regarded to consist of a single cell type, and there has been no discussion of a difference in shape between the periphery and interior of the dental epithelium (Jernvall and Thesleff, 2000; Osborn, 2008; Salazar-Ciudad and Jernvall, 2010, 2002). The present study shed light on the significance of this issue in tooth development. Our result does not require the complete discrimination of peripheral and interior cells, and is valid as long as cells in the periphery form a dense elastic sheet structure. The bending elasticity of the peripheral layer that determines the folding pattern (Fig. 3C) should correlate with the actual cell shape, cell size, and cell–cell binding in the periphery, and therefore this model relies on discontinuity in the multicellular system (Nagahara et al., 2009). By taking into account the bending elasticity at the peripheral layer, our model in its current form can not be applied to the morphological change after the appearance of the enamel knot (from E14.5 to E16 in Fig. S1A). The enamel knot is a compressed cluster of epithelial cells (Fig. 1A and B, lower panels), and should affect the mechanics in the dental epithelium; the peripheral layer can no longer be assumed to be uniform.

Our results suggest that the dental mesenchyme including the multifiber layer plays an important role in the bud-to-cap transition (Figs. 4A and B). With regard to this notion, multiple invaginations and subsequent multiple tooth formation have been observed in tooth regeneration culture, suggesting that there is a correlation between the number of invaginations and the germ size (Nakao et al., 2007). Our present study provides a working hypothesis for this observation that the tooth-germ size is critical, based on the finding that the dental mesenchyme must cover the whole epithelial bud for normal cap formation (Fig. 4B). Interestingly, we have seen that dental mesenchymal cells autonomously move to cover the dental epithelium during tooth regeneration culture (unpublished data related to (Nakao et al., 2007), and additional studies will be needed to confirm and analyze this issue in detail. Our simple model successfully reproduced the observed change in the shape of the dental epithelium even without the explicit inclusion of dental mesenchymal growth, which will be incorporated in a future study to describe the bud-to-cap transition more accurately.

The present study does not deny the contribution of chemical signaling to the bud-to-cap transition. Invagination of the dental epithelium occurs at the presumptive enamel knot expressing SHH and FGF4, which should have indispensable effects on tooth germ development. It is expected that chemical signaling and mechanical effects cooperatively realize epithelial invagination *in vivo*.

Another factor that affected the folding pattern was the p_p/p_i ratio (Fig. 3B). Interestingly, epiprofin-deficient mice that showed multiply invaginated tooth germ had delayed tooth development in the early stage, together with reduced staining for the proliferation marker PCNA (Nakamura et al., 2008). It is possible that a decrease in the intrinsic proliferation activity is related to an increase in the p_p/p_i ratio. The p_p/p_i ratio can also be considered to be correlated with the balance of migration between the periphery and interior. Further studies on cellular behavior and polarity that focus on the peripheral and interior epithelium may help to clarify the mechanism of the bud-to-cap transition.

5. Conclusions

We have demonstrated a scenario for the temporal morphological development of the tooth germ. The concept of epithelial buckling has been extended to interpret the process of the bud-to-cap transition, which has not been highlighted previously. We have presented a novel theoretical scheme in which an imbalance in the growth rates between the interior and periphery of the tissue causes a shape change. Our results suggested that the fibrous barrier between the dental mesenchyme and the oral mesenchyme plays a significant role in tooth germ development. Our simple framework of a mechanical shape change may be the basis for the incorporation of various chemical signaling processes and the actual histological geometry to more accurately describe the bud-to-cap transition in future studies.

Acknowledgments

This study was partially supported by Grants-in-Aid, KAKENHI (25103012; 15H02121). We thank Prof. Masahiro Saito (Tohoku University Graduate School of Dentistry) for his helpful comments on the process of tooth development including the formation of the multifiber layer. We acknowledge the RIKEN CDB Laboratory for Animal Resources and Genetic Engineering (Hyogo, Japan) as the source of R26R-Lyn-Venus transgenic mice (Abe et al., 2011). We also thank Yohei Nomoto, Miho Kihira, and Yousuke Nakatsu for research assistance.

Appendix A. Basic dynamics of cells

The basic dynamics for the interior epithelium were described as

$$\boldsymbol{F}^{ij} = f\left(d^{ij}_{rel}\right)\left(x^i - x^j\right) \quad \left(d^{ij}_{rel} \le d_{cutoff}\right)$$

$$\boldsymbol{F}^{ij} = 0 \quad \left(d^{ij}_{rel} > d_{cutoff}\right)$$

$$f(d) = d^{\lambda} + \frac{d_{cutoff}}{d^{\lambda}} - \left(1 + d_{cutoff}\right),$$

$$d^{ij}_{rel} = \frac{d^{ij}}{d^{ij}_0} \tag{A.1}$$

where $\boldsymbol{F}^{ij}$ is the attractive ($f<0$) or repulsive ($f>0$) force acting on cell i with respect to cell j, $\boldsymbol{x}^i$ is the position of the cell center, and d^{ij} is the distance between cell centers (Fig. 2A). We set $\lambda=2$. The optimal distance was defined as $d^{ij}_0 = r^i + r^j$, where r^i is the presumptive radius of cell i. $\boldsymbol{F}^{ij}=0$ was assumed to hold when $d^{ij}=d^{ij}_0$, and the cells were assumed to attract and repel each other when they were closer than and farther than d_0, respectively. We set the relative cutoff distance d_{cutoff}, at which interaction is lost. This corresponds to the case when the cells are apart and not in contact with each other. For interior epithelial cells, d^{inner}_{cutoff} was assigned to be $3^{1/2}$, which corresponds to the minimum distance for a non-adjacent pair in the closest-packing condition when d_0 is constant (Fig. 2D). The interaction described by Eq. (A.1) rapidly approaches zero near $d^{ij}_{rel} = d_{cutoff}$.

The motion of particles is described as,

$$\boldsymbol{x}^i_{t+1} = \boldsymbol{x}^i_t + \gamma^{-1}\sum_j k^{ij}\boldsymbol{F}^{ij}\Delta t, \tag{A.2}$$

where $\gamma^{-1}\sum_j k^{ij}\boldsymbol{F}^{ij}$ corresponds to the velocity of cell i. This assumption is based on the perspective that cells are in a very crowded environment and translational movement is relatively slow (Nagai and Honda, 2001). In the numerical simulation, a small noise was added to Eq. (A.2) to stabilize the calculation. The parameters that define the strength of cell interaction for interior-interior, interior–peripheral, and peripheral-peripheral pairs are k_{ii}, k_{ip}, and k_{pp}, respectively. The value of k_{ip} is set to be twice as great as that of k_{ii} to avoid cracking inside the modeled epithelium.

Appendix B. Cell division

The maximum cell radii of the peripheral and interior cells were assigned values of $r_{max}^{periphery}=0.5$ and $r_{max}^{inner}=1$ to represent the difference in cell density between the peripheral and interior parts of the dental epithelium. At cell division, r^i of the daughter cells is half that of the mother cell, and increases to r_{max}^i over 2500 steps. Cell division occurs at a constant probability for fully-grown cells for which $r^i=r_{max}^i$. To avoid an unrealistic cellular rearrangement accompanied by cell division, $\boldsymbol{F}_{mod}^{ij}$ was introduced as follows,

$$\boldsymbol{F}_{mod}^{ij}=m^i m^j \boldsymbol{F}^{ij},$$
$$0<m^i\le 1 \tag{B.1}$$

where m^i took a small value for daughter cells and increased from 0.1 to 1.0 over 90 steps.

When $m^i=1$ was defined for all cells at the initial state, Eq. (A.2) was revised as

$$\boldsymbol{x}_{t+1}^i=\boldsymbol{x}_t^i+\gamma^{-1}\sum_j k^{ij}\boldsymbol{F}_{mod}^{ij}\Delta t. \tag{B.2}$$

Appendix C. Peripheral layer with bending elasticity

To model peripheral cells, their relative positions were given and d_{cutoff}^{perif} was assigned a large value so that adjacent pairs always interacted with each other, except for the case of cell division. $d_0^{perif}=0.5$ was adopted instead of $d_0=1$ to represent the dense periphery and sparse interior.

To retain the smooth layering of the peripheral epithelial chain, the model included bending elasticity. It was assumed that the angle θ^{i+} formed by three successive peripheral particles i, $i+1$, and $i+2$ tended to be flat through introduction of the following force,

$$\boldsymbol{F}_{bend}^{i+}=k_{bend}\left(\boldsymbol{n}^{i+}\cos\frac{\theta^{i+}}{2}\right), \tag{C.1}$$

where $\boldsymbol{n}^{i+}$ is the unit normal vector of the vector $\boldsymbol{x}^i-\boldsymbol{x}^{i+1}$ for which $\boldsymbol{n}^{i+}\cdot(\boldsymbol{x}^{i+1}-\boldsymbol{x}^{i+2})<0$. $\boldsymbol{F}_{bend}^{i-}$ was defined for particles i, $i-1$, and $i-2$ in the same manner.

The multifiber layer was modeled with particles anchored at the initial positions. Particles in the multifiber layer were five times smaller than those in the periphery to create a dense wall.

Appendix D. Supporting information

Supplementary data associated with this article can be found in the online version at http://dx.doi.org/10.1016/j.jtbi.2015.07.006.

References

Abe, T., Kiyonari, H., Shioi, G., Inoue, K.-I., Nakao, K., Aizawa, S., Fujimori, T., 2011. Establishment of conditional reporter mouse lines at ROSA26 locus for live cell imaging. Genesis 49, 579–590.

Bilder, D., Haigo, S.L., 2012. Expanding the morphogenetic repertoire: perspectives from the Drosophila egg. Dev. Cell 22, 12–23.

Cai, J., Cho, S.-W., Kim, J.-Y., Lee, M.-J., Cha, Y.-G., Jung, H.-S., 2007. Patterning the size and number of tooth and its cusps. Dev. Biol. 304, 499–507.

Chuong, C.M., Noveen, A., 1999. Phenotypic determination of epithelial appendages: genes, developmental pathways, and evolution. J. Invest. Dermatol. Symp. Proc. 4, 307–311.

Dassule, H.R., Lewis, P., Bei, M., Maas, R., McMahon, A.P., 2000. Sonic hedgehog regulates growth and morphogenesis of the tooth. Development 127, 4775–4785.

Drasdo, D., Forgacs, G., 2000. Modeling the interplay of generic and genetic mechanisms in cleavage, blastulation, and gastrulation. Dev. Dyn. 219, 182–191.

Eiraku, M., Takata, N., Ishibashi, H., Kawada, M., Sakakura, E., Okuda, S., Sekiguchi, K., Adachi, T., Sasai, Y., 2011. Self-organizing optic-cup morphogenesis in three-dimensional culture. Nature 472, 51–56.

Fukumoto, S., Miner, J.H., Ida, H., Fukumoto, E., Yuasa, K., Miyazaki, H., Hoffman, M. P., Yamada, Y., 2006. Laminin alpha5 is required for dental epithelium growth and polarity and the development of tooth bud and shape. J. Biol. Chem. 281, 5008–5016.

Gilbert, S., 2006. Developmental Biology. Sinauer Associates Inc., Sunderland.

Gritli-Linde, A., 2002. Shh signaling within the dental epithelium is necessary for cell proliferation, growth and polarization. Development 129, 5323–5337.

Hardcastle, Z., Mo, R., Hui, C.C., Sharpe, P.T., 1998. The Shh signalling pathway in tooth development: defects in Gli2 and Gli3 mutants. Development 125, 2803–2811.

Harjunmaa, E., Kallonen, A., Voutilainen, M., Hämäläinen, K., Mikkola, M.L., Jernvall, J., 2012. On the difficulty of increasing dental complexity. Nature 483, 324–327.

Hočevar Brezavšček, A., Rauzi, M., Leptin, M., Ziherl, P., 2012. A model of epithelial invagination driven by collective mechanics of identical cells. Biophys. J. 103, 1069–1077.

Ishihara, S., Sugimura, K., 2012. Bayesian inference of force dynamics during morphogenesis. J. Theor. Biol. 313, 201–211.

Järvinen, E., Salazar-Ciudad, I., Birchmeier, W., Taketo, M.M., Jernvall, J., Thesleff, I., 2006. Continuous tooth generation in mouse is induced by activated epithelial Wnt/beta-catenin signaling. Proc. Natl. Acad. Sci. USA 103, 18627–18632.

Jernvall, J., Åberg, T., Kettunen, P., Keränen, S., Thesleff, I., 1998. The life history of an embryonic signaling center: BMP-4 induces p21 and is associated with apoptosis in the mouse tooth enamel knot. Development 125, 161–169.

Jernvall, J., Kettunen, P., Karavanova, I., Martin, L.B., Thesleff, I., 1994. Evidence for the role of the enamel knot as a control center in mammalian tooth cusp formation: non-dividing cells express growth stimulating Fgf-4 gene. Int. J. Dev. Biol. 38, 463–469.

Jernvall, J., Thesleff, I., 2000. Reiterative signaling and patterning during mammalian tooth morphogenesis. Mech. Dev. 92, 19–29.

Jussila, M., Thesleff, I., 2012. Signaling networks regulating tooth organogenesis and regeneration, and the specification of dental mesenchymal and epithelial cell lineages. Cold Spring Harb. Perspect. Biol. 4, a008425.

Kettunen, P., Karavanova, I., Thesleff, I., 1998. Responsiveness of developing dental tissues to fibroblast growth factors: expression of splicing alternatives of FGFR1, −2, −3, and of FGFR4; and stimulation of cell proliferation by FGF-2, −4, −8, and −9. Dev. Genet. 22, 374–385.

Klein, O.D., Minowada, G., Peterkova, R., Kangas, A., Yu, B.D., Lesot, H., Peterka, M., Jernvall, J., Martin, G.R., 2006. Sprouty genes control diastema tooth development via bidirectional antagonism of epithelial-mesenchymal FGF signaling. Dev. Cell 11, 181–190.

Kratochwil, K., Galceran, J., Tontsch, S., Roth, W., Grosschedl, R., 2002. FGF4, a direct target of LEF1 and Wnt signaling, can rescue the arrest of tooth organogenesis in Lef1(−/−) mice. Genes Dev. 16, 3173–3185.

Kulesa, P.M., Cruywagen, G.C., Lubkin, S.R., Maini, P.K., Sneyd, J., Murray, J.D., 1995. Modelling the spatial patterning of the teeth primordia in the lower jaw of Alligator mississippiensis. J. Biol. Syst. 3, 975–985.

Lesot, H., Brook, A.H., 2009. Epithelial histogenesis during tooth development. Arch. Oral Biol. 54 (Suppl 1), S25–S33.

Mammoto, T., Mammoto, A., Torisawa, Y.-S., Tat, T., Gibbs, A., Derda, R., Mannix, R., de Bruijn, M., Yung, C.W., Huh, D., Ingber, D.E., 2011. Mechanochemical control of mesenchymal condensation and embryonic tooth organ formation. Dev. Cell 21, 758–769.

Nagahara, H., Ma, Y., Takenaka, Y., Kageyama, R., Yoshikawa, K., 2009. Spatiotemporal pattern in somitogenesis: a non-Turing scenario with wave propagation. Phys. Rev. E 80, 021906.

Nagai, T., Honda, H., 2001. A dynamic cell model for the formation of epithelial tissues. Philos. Mag. B 81, 699–719.

Nakamura, T., de-Vega, S., Fukumoto, S., Jimenez, L., Unda, F., Yamada, Y., 2008. Transcription factor epiprofin is essential for tooth morphogenesis by regulating epithelial cell fate and tooth number. J. Biol. Chem. 283, 4825–4833.

Nakao, K., Morita, R., Saji, Y., Ishida, K., Tomita, Y., Ogawa, M., Saitoh, M., Tomooka, Y., Tsuji, T., 2007. The development of a bioengineered organ germ method. Nat. Methods 4, 227–230.

Osborn, J.W., 2008. A model of growth restraints to explain the development and evolution of tooth shapes in mammals. J. Theor. Biol. 255, 338–343.

Palacios, J., Benito, N., Berraquero, R., Pizarro, A., Cano, A., Gamallo, C., 1995. Differential spatiotemporal expression of E- and P-cadherin during mouse tooth development. Int. J. Dev. Biol. 39, 663–666.

Paus, R., Müller-Röver, S., Van Der Veen, C., Maurer, M., Eichmüller, S., Ling, G., Hofmann, U., Foitzik, K., Mecklenburg, L., Handjiski, B., 1999. A comprehensive guide for the recognition and classification of distinct stages of hair follicle morphogenesis. J. Invest. Dermatol. 113, 523–532.

Pispa, J., Thesleff, I., 2003. Mechanisms of ectodermal organogenesis. Dev. Biol. 262, 195–205.

Salazar-Ciudad, I., Jernvall, J., 2002. A gene network model accounting for development and evolution of mammalian teeth. Proc. Natl. Acad. Sci. USA 99, 8116–8120.

Salazar-Ciudad, I., Jernvall, J., 2010. A computational model of teeth and the developmental origins of morphological variation. Nature 464, 583–586.

Sasaki, T., Segawa, K., Takiguchi, R., Higashi, S., 1984. Intercellular junctions in the cells of the human enamel organ as revealed by freeze-fracture. Arch. Oral Biol. 29, 275–286.

Sherrard, K., Robin, F., Lemaire, P., Munro, E., 2010. Sequential activation of apical and basolateral contractility drives ascidian endoderm invagination. Curr. Biol. 20, 1499–1510.

Sweeton, D., Parks, S., Costa, M., Wieschaus, E., 1991. Gastrulation in Drosophila: the formation of the ventral furrow and posterior midgut invaginations. Development 112, 775–789.
Thesleff, I., 2003. Epithelial-mesenchymal signalling regulating tooth morphogenesis. J. Cell Sci. 116, 1647–1648.
Thesleff, I., Vaahtokari, A., Vainio, S., Jowett, A., 1996. Molecular mechanisms of cell and tissue interactions during early tooth development. Anat. Rec. 245, 151–161.
Toyoshima, K.-E., Asakawa, K., Ishibashi, N., Toki, H., Ogawa, M., Hasegawa, T., Irié, T., Tachikawa, T., Sato, A., Takeda, A., Tsuji, T., 2012. Fully functional hair follicle regeneration through the rearrangement of stem cells and their niches. Nat. Commun. 3, 784.
Tucker, A., Sharpe, P., 2004. The cutting-edge of mammalian development; how the embryo makes teeth. Nat. Rev. Genet. 5, 499–508.
Vaahtokari, A., Åberg, T., Jernvall, J., Keränen, S., Thesleff, I., 1996. The enamel knot as a signaling center in the developing mouse tooth. Mech. Dev. 54, 39–43.
Yoshiba, N., Yoshiba, K., Stoetzel, C., Perrin-Schmitt, F., Cam, Y., Ruch, J.V., Lesot, H., 2003. Temporospatial gene expression and protein localization of matrix metalloproteinases and their inhibitors during mouse molar tooth development. Dev. Dyn. 228, 105–112.